Optical, Electrical, and Electromechanical Properties of Hybrid Graphene/Carbon Nanotube Films

Iskandar N. Kholmanov, Carl W. Magnuson, Richard Piner, Jin-Young Kim, Ali E. Aliev, Cheng Tan, Tae Young Kim, Anvar A. Zakhidov, Giorgio Sberveglieri, Ray H. Baughman, and Rodney S. Ruoff**

Assembly of graphene with carbon nanotubes (CNTs) can yield hybrid materials with new structural characteristics and different properties than the individual components. These hybrid systems can have better functional performance compared to that of only graphene or CNTs. Graphene/CNT assemblies have been studied for the fabrication of superelastic composites,[1] ultra-flyweight aerogels,[2] high surface area materials for electrochemical energy storage,[3–6] high-efficiency electron emission sources,[7,8] electric microheaters,[9] and ultra-transparent flexible memory devices.[10] Transparent conductive films (TCF) comprising graphene/CNT assemblies have also been studied;[11–18] for these, graphene grown by chemical vapor deposition (CVD) appears particularly promising because of its better charge transfer characteristics compared, for example, to chemically modified graphene.[19,20] Charge transport of typical single-layer polycrystalline CVD-grown graphene films can be adversely affected by charge carriers scattering at various defects, including grain boundaries and line imperfections (wrinkles, folds, ripples, cracks, etc.).[21–23] In an assembly of CVD-grown graphene with CNTs, these adverse effects can be eliminated or minimized because the CNTs can provide 1D conductive paths for charge carriers and bridge the line imperfections in the graphene.[24,25] The graphene layer in these hybrid films can provide a 2D conductive platform that both fills open spaces between CNTs and connects CNTs that do not touch each other. Superior performance for graphene/CNT assemblies can perhaps be obtained through consideration of the optical, electrical, structural, and mechanical properties of both graphene and nanotubes and rational design of the hybrid material containing them.

Here, we report the dependence of the optical, electrical, and electromechanical properties of graphene/nanotube hybrid films on the type of assembly configuration. A single-layer CVD-grown graphene and a self-supporting, aligned, multiwalled carbon nanotube (MWNT) sheet (hereafter "MWNT sheet") were combined to produce hybrid films. A MWNT sheet was transferred onto CVD graphene on Cu foil to yield a MWNT sheet/graphene hybrid film as described further below. Transfer in two different arrangements (the second by simply flipping this hybrid film) yielded MWNT/graphene (MWNT/G) and graphene/MWNT (G/MWNT) hybrid films, respectively. It was observed that, despite having essentially exactly the same composition, these hybrid films exhibit different optical, electrical, and electromechanical properties. The obtained results demonstrate that high performance of these hybrid films, as compared to the separate constituents (graphene alone or MWCNT sheet alone), can be achieved by certain choices of the arrangement and combination of graphene layers and MWNT sheets.

The fabrication of MWNT/G and G/MWNT hybrid films is illustrated schematically in **Figure 1**a. Monolayer graphene was grown on polycrystalline Cu foil by chemical vapor deposition (CVD).[26] Figure 1b shows the scanning electron microscope (SEM) image of CVD-grown graphene, with wrinkles attributed to the different thermal expansions of the Cu substrate and graphene.[26] In addition, graphene on a Cu foil is not flat because it follows the surface morphology of the foil, with roughness arising from Cu grain boundaries, facets, and steps. Self-supporting, transparent, highly aligned MWNT sheets (Figure 1c) are composed of nanotubes with an average diameter of about 7–10 nm and lengths in the range of 300–400 μm. These sheets were drawn from "forests" of vertically aligned MWNTs that were grown by catalytic CVD.[27] To make the hybrid films, the MWNT sheet was placed onto a graphene monolayer supported on the Cu foil, and ethanol was then imbibed into the MWNT layer. Due to surface tension effects, the subsequent evaporation of ethanol results in densification of the MWNTs,[27] and also increases the adhesion of the MWNT film to the graphene. The Cu foil was subsequently etched in a 0.1 M ammonium persulfate ($(NH_4)_2S_2O_8$) aqueous solution yielding

Dr. I. N. Kholmanov, Dr. C. W. Magnuson, Dr. R. Piner, Dr. J.-Y. Kim, C. Tan, Dr. T. Y. Kim
Department of Mechanical Engineering
and the Materials Science and Engineering Program
University of Texas at Austin
1 University Station C2200
Austin, TX 78712, USA
E-mail: iskandar.kholmanov@austin.utexas.edu
Dr. I. N. Kholmanov, Prof. G. Sberveglieri
CNR-INO, Sensor Lab
University of Brescia
via Branze 45, 25123 Brescia, Italy
Dr. A. E. Aliev, Prof. A. A. Zakhidov, Prof. R. H. Baughman
Alan G. MacDiarmid NanoTech Institute
University of Texas at Dallas
Richardson, TX 75083-0688, USA
Prof. R. S. Ruoff
Center for Multidimensional Carbon Materials
Institute for Basic Science (IBS)
Department of Chemistry, Ulsan National Institute of Science and Technology (UNIST)
Ulsan 689798, Republic of Korea
E-mail: ruofflab@gmail.com

DOI: 10.1002/adma.201500785

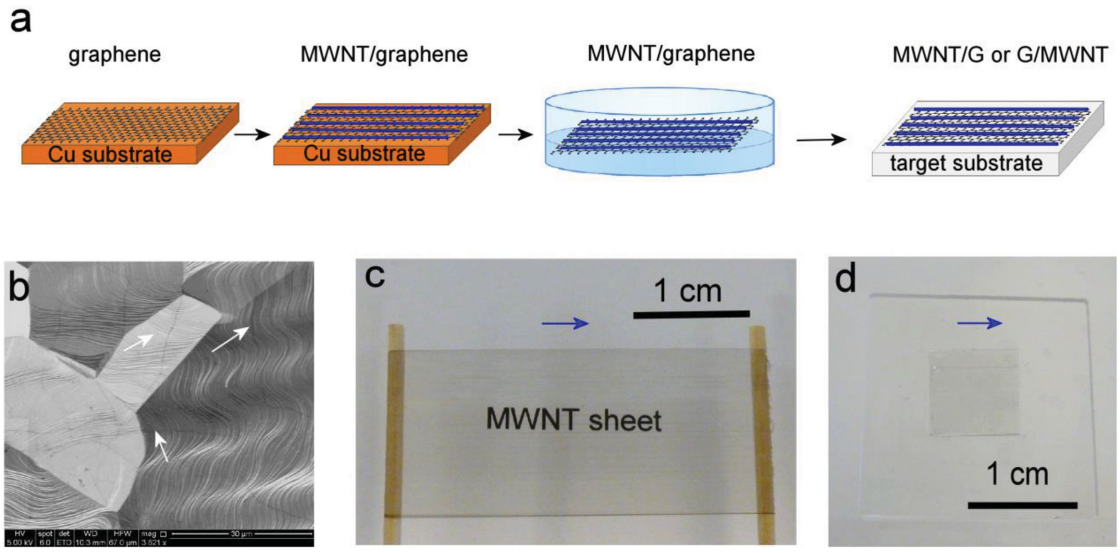

Figure 1. a) Schematic illustration of the fabrication of MWNT/G and G/MWNT hybrid films. b) SEM image of graphene grown on a polycrystalline Cu foil with grains having different surface morphologies. White arrows show graphene wrinkles. c) Photograph of a self-supporting MWNT sheet. The transparency of the sheet is evidenced by the visibility of "MWNT sheet" printed on an underlying paper. d) Photograph of a G/MWNT film on a glass substrate. Blue arrows in (c,d) show the alignment direction of MWNTs in the MWNT sheet and the G/MWNT hybrid film, respectively.

MWNT/graphene hybrid layers. Due to its self-supporting feature, the MWNT sheet allows the transfer of graphene from the Cu foil onto a target substrate without using an intermediate polymer support.[28] The obtained MWNT/graphene was directly transferred onto target substrates to fabricate MWNT/G and G/MWNT (by flipping over) hybrid films. Typical G/MWNT (Figure 1d) and MWNT/G hybrid films appear identical to the eye; however, their optical, electrical, and electromechanical properties exhibit significant differences, as described below.

Figure 2a shows an SEM image of a MWNT/G film where graphene lies on a flat SiO_2/Si substrate and MWNTs are on the top of the graphene layer. Typical line imperfections of graphene such as wrinkles or folds can be observed in these hybrid films. These defects are usually formed either during CVD growth or from the transfer processes due to the mismatch of the surface morphology between the original and final rigid substrates.[23,26] Interestingly, no such line imperfections are observed in G/MWNT films on a SiO_2/Si substrate where graphene lies on the top of the MWNTs (Figure 2b). This likely demonstrates that the MWNT sheet acts as a "soft" nonplanar support that releases structural distortions of graphene, thereby giving rise to a graphene layer with no noticeable wrinkles. This is seen from the atomic force

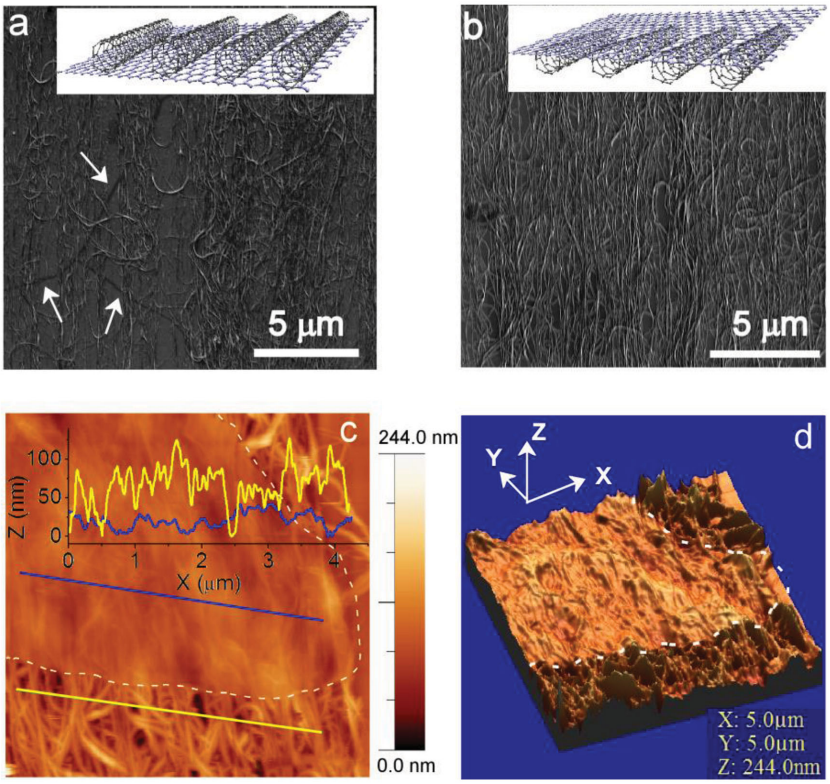

Figure 2. a) SEM image of a MWNT/G film. The inset shows schematic of the film. White arrows show the wrinkles in the graphene. b) SEM image of a G/MWNT film. The inset shows the schematic of the film. c) AFM image (5×5 μm^2) of a MWNT film partially covered with a graphene layer (a G/MWNT hybrid film). Inset curves show the line profiles of the G/MWNT (blue line) and of the pure MWNT sheet (yellow line) films. d) 3D view of (c). White dashed lines in (c) and (d) show the border of the graphene layer on the top of the MWNTs.

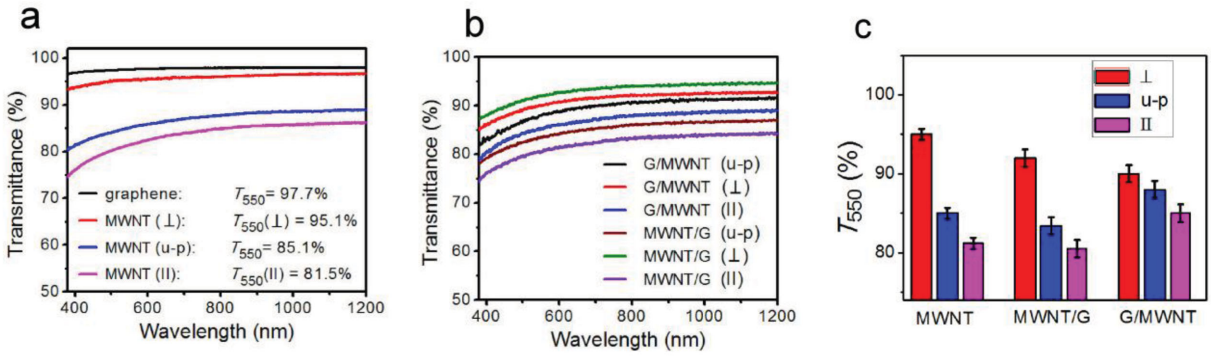

Figure 3. a) Optical transmittances of typical single-layer graphene and MWNT sheet on glass substrate. Since films composed of aligned MWNTs have anisotropy, the optical transmittances for incident light polarized parallel ($T(\|)$) and perpendicular ($T(\perp)$) to the alignment direction of the nanotubes, and for un-polarized (u-p) (T) light radiation are shown. b) Optical transmittance of typical MWNT/G and G/MWNT films for polarized and u-p light radiation is shown. c) Bar graph comparison of T_{550} for a single MWNT sheet and for MWNT/G and G/MWNT films, showing the lower anisotropy for the hybrid films compared to the pure MWNT film.

microscope (AFM) image (Figure 2c and inset curves) of a graphene layer on the top of the MWNT sheet layer. When covered by the monolayer of graphene the MWNT sheet undergoes substantial change in its morphology, behaving as a "soft substrate." Graphene flattens the MWNT sheet by converting the "out-of-plane deviations" in the sheet into in-plane structures (Figure 2d). This decreases the average thickness of the MWNT sheet to 17 ± 1.15 nm, almost three times smaller than the average thickness of the MWNT sheet (55 ± 3.75 nm) with no graphene coverage. Graphene on the top of MWNTs lowers the root-mean-square (rms) roughness of the MWNT sheet from about 64.7 nm for pure MWNT films to about 17.5 nm for G/MWNT films. No such densification and surface morphology changes have been observed in MWNT/G films; thus, we find that the graphene layer for that configuration does not affect the morphology of the MWNT sheets. These dissimilarities in structural characteristics between the MWNT/G and G/MWNT films result in differences in their optical, electrical and electromechanical properties, as shown below.

Figure 3a shows the optical transmittance of typical individual graphene and MWNT sheets supported on glass substrates, where the subscript on transmittance T indicates the measurement wavelength in nanometer. For these measurements, ethanol was imbibed into the MWNT sheet after adhering it to the substrate, and subsequently evaporated, resulting in densification and a better adhesion of the sheet to the substrate. Graphene is optically isotropic with T_{550} = 97.7 ± 0.04%. In contrast, the MWNT sheets exhibit anisotropy, with T_{550} = 85.1 ± 0.5% for unpolarized light, $T_{550}(\|)$ = 81.5 ± 0.5% for light polarized parallel to the nanotube alignment direction, and $T_{550}(\perp)$ = 95.1 ± 0.5% for light that is polarized orthogonally.

The optical transmittances of the typical MWNT/G and G/MWNT films are shown in Figure 3b. Both hybrid films show anisotropy in optical transmittance that can be ascribed to the presence of aligned MWNTs. However, the hybrid films exhibit lower anisotropy compared to the pure MWNT film. Typically, for pure MWNT sheets with T_{550} = 85 ± 0.9% (for unpolarized light), the difference between ⊥ and ∥ components ($T_{550}(\perp) - T_{550}$(ii)) is about 14%, while in the MWNT/G and G/MWNT films this difference is in the range of 11%–13% and 4%–6%, respectively (Figure 3c).

For both polarized (⊥ and ∥) and unpolarized light the optical transmittance of the MWNT/G hybrid films is lower than that of the corresponding pure MWNT sheets (Figure 3c), as is anticipated. G/MWNT hybrid films have higher (when it could be expected to be lower) optical transmittance for ∥-polarized and unpolarized light, compared to that of pure MWNT films. This transmittance of the G/MWNT hybrid films does not obey the general rule for multilayer systems that is $T_{total} = T_{graphene} \times T_{MWNT}$, [29] where $T_{graphene}$ and T_{MWNT} are the percent of light transmission of pure graphene and MWNT layers, respectively, and T_{total} is the percent of light transmission for the G/MWNT stack. In addition, G/MWNT films have lower anisotropy in comparison to both the MWNT sheet and the MWNT/G films. We suggest that the optical characteristics of the G/MWNT films can be ascribed to the structural modification of the MWNT sheet from it being covered by a graphene layer. Zhang et al.[27] previously demonstrated that the transmittance of the aligned MWNT sheets for ∥-polarized and unpolarized light increases after their liquid-based densification. Similarly, for the G/MWNT films, MWNTs misaligned out of the sheet plane can be pressed into the sheet plane by the top graphene layer, as observed in AFM images (Figure 2c,d). This change in the morphology (densification) of the MWNT sheet results in increased optical transmittance for ∥-polarized and unpolarized light and in decreased in-plane optical anisotropy. No such structural changes were observed in the MWNT/G film and so its optical properties are different from that of the G/MWNT film.

Figure 4a shows a plot of sheet resistance for MWNT sheets, MWNT/G and G/MWNT films, and single-layer graphene films. The hybrid films have significantly lower sheet resistance than single-layer graphene and pure MWNT films. Due to the alignment of MWNTs, the MWNT sheets and the hybrid films have anisotropic transport with the lowest sheet resistance along the direction parallel to nanotube alignment ($R_s(\|)$). Pure MWNT films have higher anisotropy ($R_s(\|)$ = 710 ± 54 Ω sq^{-1} and $R_s(\perp)$ 9.4 ± 1.02 kΩ sq^{-1}), compared to MWNT/G

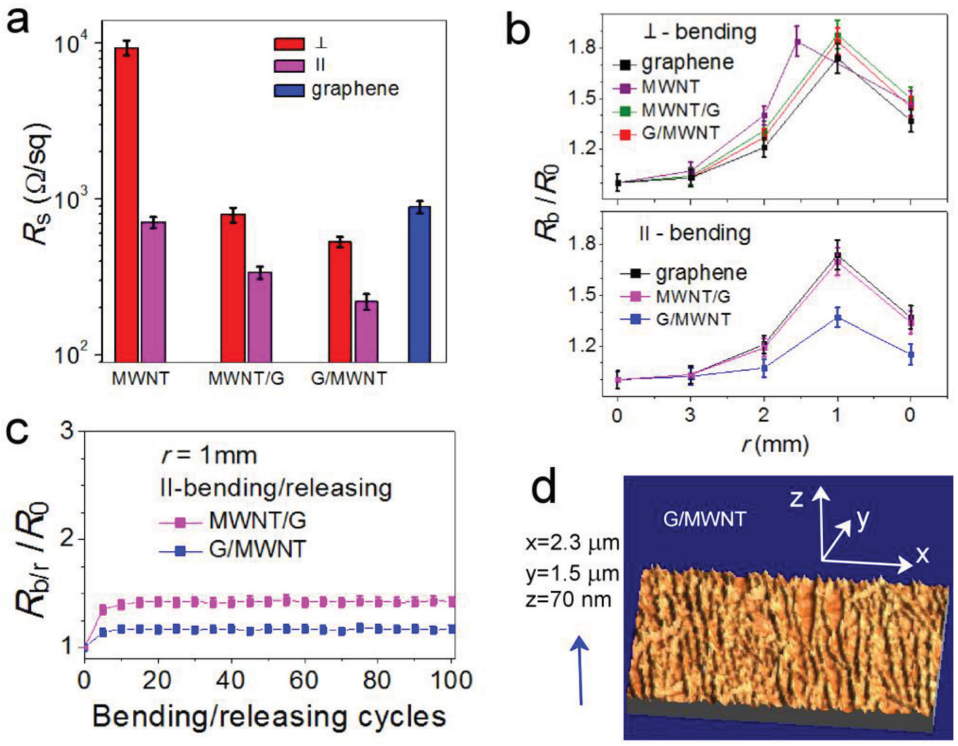

Figure 4. a) Bar view illustration of sheet resistances of MWNT, MWNT/G, and G/MWNT films measured along (∥) and perpendicular (⊥) to the nanotube alignment direction. The sheet resistance of a graphene film is also shown. b) Variation of the electrical resistance (R_b/R_0), in the direction of applied tensile strain, of MWNT, MWNT/G, and G/MWNT films for bending along the axis perpendicular (top) and parallel (bottom) to the direction of nanotube alignment. c) Resistance changes ($R_{b/r}/R_0$) under bending/releasing cycles along the axis parallel to the direction of nanotube alignment for a bending radius of 1 mm. d) 3D AFM image of a G/MWNT hybrid film. The blue arrow shows the nanotube alignment direction.

($R_s(\|)$ = 337 ± 31 Ω sq^{-1}, $R_s(\perp)$ 804 ± 87 Ω sq^{-1}), and G/MWNT ($R_s(\|)$ = 220 ± 30 Ω sq^{-1}, $R_s(\perp)$ 530 ± 41 Ω sq^{-1}) hybrid films. The G/MWNT films have the lowest sheet resistances. In G/MWNT films, the compression of the MWNT sheet by the top graphene layer likely improves and/or increases the number of the nanotube-nanotube junctions, creating better and/or additional channels for charge transport in both the ∥ and ⊥ directions.

The changes in electrical resistance under mechanical bending (R_b/R_0, where R_0 is the initial resistance in a flat state and R_b is the resistance in a bent state) were tested for MWNT sheets, graphene, MWNT/G films, and G/MWNT films deposited onto 300 μm thick poly(ethylene terephthalate) (PET) substrates. Figure 4b shows the changes of resistances measured in the direction of applied tensile strain (the resistance changes in the direction perpendicular to the tensile strain that are almost invariant are not shown). Under bending along the axis perpendicular to the nanotube alignment direction, the pure MWNT films exhibit only small changes in resistance up to a bending radius of r = 3 mm (approximate tensile strain of 5%). When decreasing the bending radius below 3 mm, the resistance of the nanotube films starts to dramatically increase, and nearly doubled R_b/R_0 at r = 1.55 mm (approximate tensile strain of 10%) (Figure 4b, top). For this bending direction, MWNT/G and G/MWNT hybrid films have similar changes in resistance of 1.88 ± 0.08 and 1.84 ± 0.08 at r = 1 mm (tensile strain 15%), respectively. Both hybrid films exhibit slightly larger changes in resistance compared to pure graphene (R_b/R_0 = 1.74 ± 0.08 in r = 1 mm; Figure 4b, top).

In contrast, under bending along the axis parallel to the nanotube alignment, the MWNT/G and G/MWNT hybrid films show different changes in resistance (Figure 4b, bottom). Under this bending direction, pure MWNT films display large resistance changes with R_b/R_0 = 2.50 ± 0.70 for r = 3 mm (not shown). The MWNT/G films have changes in resistance (R_b/R_0 = 1.71 ± 0.07 for r = 1 mm) similar to that of graphene films, demonstrating that the electrical conductivity in this direction is mainly contributed by the graphene films. The G/MWNT hybrid films have significantly smaller (R_b/R_0 = 1.37 ± 0.05 in r = 1 mm) changes in resistance. When released after first bending to a radius of r = 1 mm, the resistance ($R_{b/r}$—resistance after a bending/releasing cycle) of MWNT/G hybrid films increases to about 1.35R_0, while in G/MWNT films it increases to 1.14R_0. After two to three bending/releasing cycles, the films display stable $R_{b/r}$ values, as shown in Figure 4c.

The superior electromechanical properties of G/MWNT films can be ascribed to certain aspects of the morphology of such films. The MWNT sheets were found to have an array of "grooves," that graphene, due to its low flexural rigidity (EI ≈ 1.1 × 10^{-19} J/per unit width),[30] can conform to (in some degree), yielding a "wavy" morphology in the G/MWNT films (Figure 4d). We suggest that during bending such "wavy" structures can undergo deformations that result in changes in amplitudes and wavelengths, and result in better electromechanical

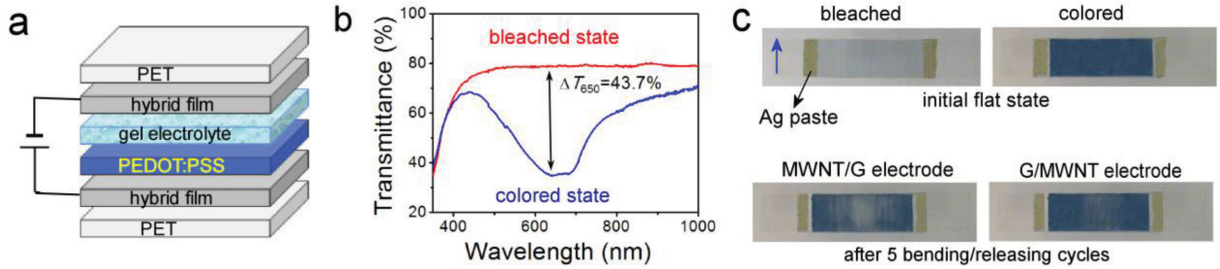

Figure 5. a) A schematic structure of the EC device with hybrid films (MWNT/G or G/MWNT) as transparent electrodes. b) Optical transmittance spectra of the flat EC device at colored and bleached states, with the highest absorption wavelength of the colored state at 650 nm. c) Photographs of a flat EC device in bleached and colored states (top), and in colored states after five bending/releasing cycles (to and from a curvature radius of 1 mm) of the EC device with MWNT/G (bottom left) and G/MWNT (bottom right) electrodes. The blue arrow shows the alignment direction of MWNTs in the hybrid film. The size of the colored area in the EC devices is about 1.5×0.5 cm^2.

properties of G/MWNT films compared to MWNT/G hybrid films in which graphene lies on a flat substrate. In addition, "flattening," "buckling" and "kinking" deformations in nanotubes may contribute to the high flexibility of the hybrid films.[31,32]

G/MWNT and MWNT/G hybrids were tested as transparent electrodes in electrochromic devices. The hybrid films on 300 μm thick PET substrates were integrated into an electrochromic (EC) device (**Figure 5**a), in which conducting p-doped polymer poly(3,4-ethylenedioxythiophene) with a poly(styrene sulfonate) (PEDOT:PSS) copolymer was used as an active EC material. Ion gel composed of poly(vinylidene fluoride-co-hexafluoropropylene), P(VDF-HFP), ionic liquid (1-ethyl-3-methylimidazolium bis(trifluoromethylsulfonyl) amide, [EMI][TFSA]),[33] and mixed with $LiClO_4$ was used as the gel electrolyte.

The operation principle of the EC device, schematically illustrated in Figure 5a, is based on the reversible modulations in the optical properties of PEDOT due to redox reactions under applied external voltages. A negative voltage (–2.7 V) applied to the transparent electrode in contact with the EC layer causes injection of electrons and the intercalation of Li^+ ions, resulting in the reduction of the PEDOT. This leads to an intense optical absorption of the visible light (with absorption peak at wavelengths centered at about 650 nm (Figure 5b)), providing a blue color to the EC layer. Application of a reverse external voltage (2.1 V) results in oxidation of the PEDOT. In the bleached state, the optical properties of PEDOT are determined by the transitions between bipolaronic states that have low optical absorption in the visible wavelength regions.[34]

The EC devices with both G/MWNT and MWNT/G transparent electrodes in flat states exhibit stable coloration (T_c = 35% at 650 nm) and bleaching (T_b = 78.7% at 650 nm) with an optical contrast of $\|T$ ($T_b - T_c$) = 43.7% at 650 nm and with the coloration and bleaching times of 25 s and 17 s, respectively (Figure 5b,c, top images). Stable optical modulations up to 100 coloration/bleaching cycles were found during testing.

However, for bending to a 1 mm curvature radius, along the axis parallel to the MWNT alignment direction, the EC devices with G/MWNT and MWNT/G electrodes display different optical modulations. Figure 5c (bottom left image) shows the EC device with MWNT/G transparent electrodes in the colored state after five bending/releasing cycles. In the central part (highest bending curvature) of the device, the optical contrast between coloration and bleaching states decreases to about $\| T$ = 8.5%, which is similar to that of EC devices with pure graphene transparent electrodes (not shown). In contrast, EC devices with G/MWNT electrodes after the same bending–releasing cycles maintain significantly higher optical contrast (ΔT = 21.7%) (Figure 5c, bottom right). The difference in the optical contrast between the EC devices can be attributed to the better electromechanical properties of the G/MWNT films, compared to the MWNT/G films. This shows that the performance of the hybrid films depends on the assembly arrangement of the graphene and MWNT layers in the hybrid films. We note that when using pure MWNT transparent electrodes in EC devices with the configuration shown in Figure 5a no homogenous coloration has been obtained in flat state, and after first bending/releasing cycle only edges near the Ag electrodes were colored, while the main part of the device remained bleached.

The obtained results demonstrate that although the G/MWNT and MWNT/G are from the same initial film removed from the Cu foil, their optical, electrical, and electromechanical properties differ due to changes in structure that occur in the G/MWNT configuration, when it is adhered to different substrates. Although the weight fraction of the graphene sheet in the hybrid films is very low, since the nanotube/graphene weight ratio is estimated to be 27 ± 1.03 (see the Supporting Information), the graphene layer can yield substantial morphological changes in the MWNT films by converting the "out-of-plane" nanotubes into in-plane structures within the MWNT film. These changes affect the optical, electrical, and electromechanical properties of G/MWNT films, making them different from MWNT/G films. Note that the electrical conductivity of the hybrid films could be increased by replacing the presently used MWNT sheets with forest-drawn sheets of few wall nanotubes and by doping both the graphene and nanotubes, making them more suitable for transparent electrode applications.

In summary, by adhering a MWNT sheet containing aligned MWNTs to a CVD grown graphene layer on copper foil, and then by releasing the resulting "MWNT/G film" from the Cu foil, it is possible to achieve two different configurations, namely MWNT/G and G/MWNT films having the same composition. When graphene is on the top of the "MWNT sheet" layer (i.e., the G/MWNT configuration), it significantly modifies the MWNT sheet giving rise to better electrical, optical, and electromechanical responses than the MWNT/G configuration,

with both of the hybrid film configurations typically showing better response than MWNT sheet or graphene (G) alone. In the same sense, the graphene is modified when on the MWNT sheet in that wrinkles and "folds" are observed to be "released" and thus removed by this highly porous and compliant substrate. The results demonstrate that high performance of these hybrid films, as compared to the separate constituents, can be achieved by certain choices of the arrangement and combination of graphene layers and MWNT sheets. These studies have important implications for further research on all-carbon hybrid films and indicate their high potential in a broad range of applications including flexible, displays, photovoltaics, and organic light-emitting diodes.

Experimental Section

Fabrication of Graphene, MWNT Sheet, and G/MWNT/G Hybrid Films: Monolayer graphene was grown on thick (25 μm), polycrystalline Cu foils using chemical vapor deposition (CVD), as described elsewhere.[26] An aligned self-supporting MWNT sheet (Figure 1c) was put on the top of the graphene/Cu foil. Ethanol was then imbibed into the sample to densify the MWNTs during subsequent ethanol evaporation.[27] This increases the adhesion of the MWNT film to the graphene/Cu substrate. The sample was annealed at 100 °C for 10 min on a hot plate under normal atmosphere. After etching the Cu foil in the ammonium persulfate ($(NH_4)_2S_2O_8$) (0.1 M) aqueous solution, the free-standing MWNT/graphene was rinsed with distilled water five to seven times. Next, the MWNT/graphene was transferred onto target substrates to form MWNT/G or (by flipping over) G/MWNT hybrid films. Since the concentration of metal catalyst particles in the MWNT sheets is at most 2.8 wt% (see Supporting Information and Figure S1), this low impurity concentration is expected to have little effect of measured properties for the MWNT films and the hybrid films.

The sheet resistance of the films was measured using in-line four probe methods. The four Au contacts (each with dimensions of 40 × 40 μm^2 to minimize the potential influence of local inhomogeneities in the MWNT film density/structure) were deposited by e-beam evaporation using a metal mask. The experimental data were averaged over measurements of 24 hybrid films and 8, 4, 1.6, and 1.2 mm spacing between contacts. The contacts were deposited parallel or perpendicular to the MWNT alignment direction in the films.

Optical transmittances of the samples were measured using a Cary 5000 Ultraviolet-Visible-Near infrared spectrometer. The optical transmittance spectra of (i) graphene films was acquired for four samples, and for (ii) MWNT, G/MWNT, and MWNT/G films, eight samples of each were measured. The experimental data shown in Figure 3c was obtained by averaging the transmittance spectra of eight samples of each (MWNT, G/MWNT, and MWNT/G films).

The average thickness of each sample was obtained from the AFM mapping data by averaging the data for five samples of each type (MWNT, G/MWNT, and MWNT/G films).

Preparation of an Ion-Gel Electrolyte for Electrochromic (EC) Devices: Ion gels based on poly(vinylidene fluoride-*co*-hexafluoropropylene), P(VDF-HFP), and ionic liquid (1-ethyl-3-methylimidazolium bis(trifluoromethylsulfonyl) amide, [EMI][TFSA]) were prepared by dissolving these two components together in acetone with a weight ratio of 1:4:7 between polymer, ionic liquid, and solvent, as described elsewhere.[33] $LiClO_4$ powder was added to the solution (with a concentration of 1 M with respect to [EMI][TFSA]) and stirred for 10 min at room temperature. The obtained gel electrolyte has Li^+ ions that contribute to the ionic conductivity of the electrolyte.

G/MWNT and MWNT/G hybrid films on PET substrates were used as transparent electrodes in EC devices. In each device two same type (either G/MWNT or MWNT/G) hybrid films were used: one as a top and another as a bottom transparent electrode, as shown in Figure 5a. Ag paste was smeared at the edges of electrodes and was used to apply an external electric field to the device for its optical modulations. Electrochromic p-doped polymer poly(3,4-ethylenedioxythiophene) with poly(styrene sulfonate) (PEDOT:PSS) copolymer was used as the active EC material. In order to have better adhesion on the transparent electrodes, a solution of PEDOT:PSS was mixed with ethyl cellulose (0.1 M) in ethanol at a 1:1 volume ratio. The EC mixture was deposited onto one of the two same type transparent electrodes by drop casting and dried for 5 min under ambient conditions. The gel electrolyte (about 70 μm thick) was then deposited on the top of the EC layer by drop casting and kept at 50 °C for 1 h under ambient atmosphere. Another transparent electrode on a PET substrate was put on the top of the gel electrolyte and delicately pressed to obtain a good contact with the electrolyte. A transparent scotch tape was used to fix the sandwiched EC devices.

Supporting Information

Supporting Information is available from the Wiley Online Library or from the author.

Acknowledgements

This work was supported by the National Science Foundation (Grant No. DMR 1206986), by Air Force Office of Scientific Research grant FA9550-12–1-0211, and by Welch Foundation grant AT 16-17. R.S.R. was supported by IBS-R019-D1.

Received: February 13, 2015
Revised: March 26, 2015
Published online: April 11, 2015

[1] K. H. Kim, Y. Oh, M. F. Islam, *Nat. Nanotechnol.* **2012**, *7*, 562.
[2] H. Sun, Z. Xu, C. Gao, *Adv. Mater.* **2013**, *25*, 2554.
[3] D. Yu, K. Goh, H. Wang, L. Wei, W. Jiang, Q. Zhang, L. Dai, Y. Chen, *Nat. Nanotechnol.* **2014**, *9*, 555.
[4] C. Tang, Q. Zhang, M. Q. Zhao, J. Q. Huang, X. B. Cheng, G. L. Tian, H. J. Peng, F. Wei, *Adv. Mater.* **2014**, *26*, 6100.
[5] M. Q. Zhao, X. F. Liu, Q. Zhang, G. L. Tian, J. Q. Huang, W. Zhu, F. Wei, *ACS Nano* **2012**, *6*, 10759.
[6] D. T. Pham, T. H. Lee, D. H. Luong, F. Yao, A. Ghosh, V. T. Le, T. H. Kim, B. Li, J. Chang, Y. H. Lee, *ACS Nano* **2015**, *9*, 2018.
[7] D. H. Lee, J. E. Kim, T. H. Han, J. W. Hwang, S. Jeon, S. Y. Choi, S. H. Hong, W. J. Lee, R. S. Ruoff, S. O. Kim, *Adv. Mater.* **2010**, *22*, 1247.
[8] F. Tristan-Lopez, A. Morelos-Gomez, S. M. Vega-Diaz, M. L. Garcia-Betacourt, N. Perea-Lopez, A. L. Elias, H. Muramatsu, R. Cruz-Silva, S. Tsuruoka, Y. A. Kim, T. Hayahsi, K. Kaneko, M. Endo, M. Terrones, *ACS Nano* **2013**, *7*, 10788.
[9] P. Xiao, C. Wan, J. Gu, Z. Liu, Y. Men, Y. Huang, J. Zhang, L. Zhu, T. Chen, *Adv. Funct. Mater.* **2015**, DOI: 10.1002/adfm.201404624.
[10] W. J. Yu, S. H. Chae, S. Y. Lee, D. L. Duong, Y. H. Lee, *Adv. Mater.* **2011**, *23*, 1889.
[11] V. C. Tung, L. M. Chen, M. J. Allen, J. K. Wassei, K. Nelson, R. B. Kaner, Y. Yang, *Nano Lett.* **2009**, *9*, 1949.
[12] P. J. King, U. Khan, M. Lotya, S. De, J. N. Coleman, *ACS Nano* **2010**, *4*, 4238.
[13] D. D. Nguyen, N. H. Tai, S. Y. Chen, Y. L. Chueh, *Nanoscale* **2012**, *4*, 632.
[14] Y. K. Kim, D. H. Min, *Langmuir* **2009**, *25*, 11302.
[15] Z. Yan, Z. Peng, G. Casillas, J. Lin, C. Xiang, H. Zhou, Y. Yang, G. Ruan, A. R. O. Raji, E. L. G. Samuel, R. H. Hauge, M. J. Yacaman, J. M. Tour, *ACS Nano* **2014**, *8*, 5061.

[16] T. K. Hong, D. W. Lee, H. J. Choi, H. S. Shin, B. S. Kim, *ACS Nano* **2010**, *4*, 3861.
[17] B. R. Lee, J. S. Kim, Y. S. Nam, H. J. Jeong, S. Y. Jeong, G. W. Lee, J. T. Han, M. H. Song, *J. Mater. Chem.* **2012**, *22*, 21481.
[18] X. Lin, P. Liu, Y. Wei, Q. Li, J. Wang, Y. Wu, C. Feng, L. Zhang, S. Fan, K. Jiang, *Nat. Commun.* **2013**, *4*, 2920.
[19] K. S. Kim, Y. Zhao, H. Jang, S. Y. Lee, J. M. Kim, K. S. Kim, J. H. Ahn, P. Kim, J. Y. Choi, B. H. Hong, *Nature* **2009**, *457*, 706.
[20] S. Bae, H. Kim, Y. Lee, X. Xu, J. S. Park, Y. Zheng, J. Balakrishnan, T. Lei, H. R. Kim, Y. I. Song, Y. J. Kim, K. S. Kim, B. Ozyilmaz, J. H. Ahn, B. H. Hong, S. Iijima, *Nat. Nanotechnol.* **2010**, *5*, 574.
[21] O. V. Yazyev, S. G. Louie, *Nat. Mater.* **2010**, *9*, 806.
[22] P. Y. Huang, C. S. Ruiz-Vargas, A. M. van der Zande, W. S. Whitney, M. P. Levendorf, J. W. Kevek, S. Garg, J. S. Alden, C. J. Hustedt, Y. Zhu, J. Park, P. L. McEuen, D. A. Muller, *Nature* **2011**, *469*, 389.
[23] G. X. Ni, Y. Zheng, S. Bae, H. R. Kim, A. Pachoud, Y. S. Kim, C. L. Tan, D. Im, J. H. Ahn, B. H. Hong, B. Ozyilmaz, *ACS Nano* **2012**, *6*, 1158.
[24] S. H. Kim, W. Song, M. W. Jung, M. A. Kang, K. Kim, S. J. Chang, S. S. Lee, J. Lim, J. Hwang, S. Myung, K. S. An, *Adv. Mater.* **2014**, *26*, 4247.
[25] C. Li, Z. Li, H. Zhu, K. Wang, J. Wei, X. Li, P. Sun, H. Zhang, D. Wu, *J. Phys. Chem. C* **2010**, *114*, 14008.
[26] X. Li, W. Cai, J. An, S. Kim, J. Nah, D. Yang, R. Piner, A. Velamakanni, I. Jung, E. Tutuc, S. K. Banerjee, L. Colombo, R. S. Ruoff, *Science* **2009**, *324*, 1312.
[27] M. Zhang, S. Fang, A. A. Zakhidov, S. B. Lee, A. E. Aliev, C. D. Williams, K. R. Atkinson, R. H. Baughman, *Science* **2005**, *309*, 1215.
[28] I. N. Kholmanov, C. W. Magnuson, A. E. Aliev, H. Li, B. Zhang, J. W. Suk, L. L. Zhang, E. Peng, S. H. Mousavi, A. B. Khanikaev, R. Piner, G. Shvets, R. S. Ruoff, *Nano Lett.* **2012**, *12*, 5679.
[29] C. Jeong, P. Nair, M. Khan, M. Lundstrom, A. M. Alam, *Nano Lett.* **2011**, *11*, 5020.
[30] Y. Huang, J. Wu, K. C. Hwang, *Phys. Rev. B: Condens. Matter* **2006**, *74*, 245413.
[31] R. S. Ruoff, J. Tersoff, D. C. Lorents, S. Subramoney, B. Chan, *Nature* **1993**, *364*, 514.
[32] D. Qian, G. J. Wagner, W. K. Liu, M. F. Yu, R. S. Ruoff, *Appl. Mech. Rev.* **2002**, *55*, 495.
[33] K. H. Lee, M. S. Kang, S. Zhang, Y. Gu, T. P. Lodge, C. D. Frisbie, *Adv. Mater.* **2012**, *24*, 4457.
[34] P. Andersson, D. Nilsson, P.-O. Svensson, M. Chen, A. Malmström, T. Remonen, T. Kugler, M. Berggren, *Adv. Mater.* **2002**, *14*, 1460.